Macromolecules
ARTICLE

Macromolecules **2009**, *42*, 7439–7446 **7439**
DOI: 10.1021/ma901504h

Heat-Set Poly(ethylacrylic acid) Nanoparticles: Combined Light Scattering, Calorimetric, and FTIR Study

Marián Sedlák,*,† Čestmír Koňák,‡ and Jiří Dybal‡

†*Institute of Experimental Physics, Slovak Academy of Sciences, Watsonova 47, 040 01 Košice, Slovakia, and* ‡*Institute of Macromolecular Chemistry, Academy of Sciences of the Czech Republic, Heyrovsky Sq. 2, 162 06 Prague 6, Czech Republic*

Received May 6, 2009; Revised Manuscript Received August 12, 2009

ABSTRACT: Stable polymeric nanoparticles were prepared by self-assembly of poly(ethylacrylic acid) homopolymers. The mechanism of the self-assembly is based on heating a solution of thermoresponsive partially charged PEA with subsequent stabilization of particles by hydrogen bonds between polymer chains. Thermoresponsivity is tuned by the polymer degree of ionization. A deeper insight into the mechanism of the self-assembly is brought by a combination of static, dynamic, and electrophoretic light scattering with calorimetry and FTIR spectroscopy. The full irreversibility and the width of the transition as seen by scattering methods are confirmed also by differential scanning calorimetry. As revealed by FTIR measurements, the irreversibility of the nanoparticle formation is achieved by their stabilization via hydrogen bonds, mainly $COOH\cdots COO^-$. The mechanism of the stabilization of PEA nanoparticles comprised of charged chains by a concerted action of hydrophobic and hydrogen bond interactions reminds of the situation in globular proteins. Similarly to globular proteins, PEA nanoparticles can be denatured by urea.

Introduction

A new approach to polymer self-assembly was presented in the preceding paper.[1] Stable polymeric nanoparticles were prepared from homopolymers of one type only (poly(ethacrylic acid)) and without any assembly triggering additives. The self-assembly was based on the following idea. A thermosensitive polymer solution is heated, the solvent quality worsens, and polymer chains are forced to associate. The irreversibility of this association is presumably achieved such that chains getting into a close proximity become hydrogen bonded. As a result, nanoparticles do not dissolve upon cooling to ambient temperature and remain stable. Charges on chains yield a moderate zeta potential of resulting nanoparticles and ensure their stability.

The size of PEA nanoparticles can be monitored during the growth by light scattering techniques and can be custom-tailored by tuning critical parameters, especially the temperature and time of heating. Obtained nanoparticles are stable over long periods of time. They are stable in a broad range of salt concentrations, including physiological conditions, and possess a mild acceptable degree of polydispersity.

The aim of the current paper is to obtain a more complex information on the molecular mechanism of the self-assembly by a combination of scattering techniques, calorimetry, and FTIR spectroscopy. In a sense, the paper verifies and confirms the premises on which the above-mentioned route to the preparation of stable polymeric nanoparticles was originally designed.

Experimental Section

Material. Poly(ethylacrylic acid), $M_w = 18\,600$, $M_n = 12\,400$, and $M_w/M_n = 1.5$, was obtained from Polymer Source, Canada, and used as delivered. The moisture content in the bulk polymer was established by the Karl Fischer method and taken into account in the preparation of exact concentrations. Low molar mass substances were of analytical grade (Merck, Darmstadt). Water was freshly double-distilled in a quartz apparatus and subsequently deionized by analytical grade mixed-bed ion exchange resins (Bio-Rad, Richmond, CA). The resistivity of water was above 15 MΩ cm.

Static Light Scattering. The static light scattering (SLS) as well as dynamic light scattering (DLS) measurements were made using a Stabilite 2017-04S argon laser (Spectra Physics, Mountain View, CA) with 514.5 nm vertically polarized beam. Laser power was limited to 100 mW maximum via neutral density filters. A laboratory made goniometer with angular range from 30° to 150° was used to collect data for both static and dynamic light scattering experiments. The scattering cell was thermostated at 25 °C with a precision of ±0.1 °C. All solutions were filtered through 0.2 μm filters. Scattering intensities were measured by photon counting. Solvent scattering was subtracted from total solution scattering to obtain excess scattering intensity. A distilled benzene standard was used for the scattering intensity normalization. Scattering intensities are normalized throughout the work as ratios I/I_B, where I_B is benzene scattering.

Dynamic Light Scattering. An ALV-5000/E correlator with a fast correlation board option (ALV, Langen, Germany) was used for photon correlation measurements. Characteristic decay times of dynamic modes τ_i and their relative amplitudes $A_i(\tau_i)$ were evaluated through the moments of distribution functions of decay times $A(\tau)$ obtained by fitting correlation curves using CONTIN[2] and GENDIST[3,4] programs. Diffusion coefficients were calculated as $D_i = (1/\tau_i)q^{-2}$.

pH Titrations. An MPT-2 autotitrator model ZEN1001 (Malvern Instruments) was used for pH measurements. The electrode system was calibrated with pH standards (Aldrich) 4, 7, and 9, prior to each titration. All titrations were performed under a nitrogen atmosphere at 25 °C in closed titration vessels filled with 7 mL of solution of PEA nanoparticles ($c = 0.033$ g/kg) under constant stirring. The titrants were 0.01 mol/L solutions of HCl or NaOH obtained from Aldrich, which were added at a rate 6 mL/h. A 25 min delay was allowed

*Corresponding author. E-mail: marsed@saske.sk.

© 2009 American Chemical Society

Published on Web 09/11/2009

between additions, in order to ensure that the acid−base reaction has reached the equilibrium.

Electrophoretic Light Scattering. Zeta potentials (ζ) were measured using a Nano-ZS, Model ZEN3600 (Malvern Instruments, UK) equipped with a He−Ne laser operating at a wavelength of 632.8 nm. The zeta potential was measured at least 10 times to check for repeatability. The measured electrophoretic mobilities [μm cm (V s)$^{-1}$] were converted to zeta potential (mV) using the Smoluchowski approximation. A reference measurement using the Malvern zeta potential standard was run prior to each sample analysis to check the correct instrument operation. Concurrent DLS measurements during pH titration were performed also by a Malvern Nano-ZS, Model ZEN3600, working at scattering angle 173°. Since diffusion coefficient is angularly dependent,[1] obtained apparent hydrodynamic radii are somewhat smaller than those calculated from zero angle extrapolated diffusion coefficients.

Differential Scanning Calorimetry (DSC) measurements were performed on the Perkin-Elmer Pyris 1 DSC calorimeter. Samples of about 5 mg were closed in Al sample pans, and the system was flushed with dry helium during the DSC scan. The temperature scale was calibrated according to the melting points of cyclohexane and indium. The power output scale was calibrated with indium. The samples were scanned in the temperature interval from 21 to 81 °C. Measurements in the standard DSC mode were performed with constant heating rate 1 °C/min in heating and cooling runs. There was a hold for 3 min at 81 °C between the heating and cooling run.

FTIR Spectroscopy. ATR FTIR spectra were collected on a Nicolet Nexus 870 FTIR spectrometer purged with dry air and equipped with a cooled mercury−cadmium−telluride (MCT) detector. Samples were measured on a horizontal micro-ATR Golden Gate unit (SPECAC) with a diamond prism; spectral resolution was 4 cm^{-1}. All the spectra were processed by ATR correction.

Quantum Chemical Calculations. The model calculations were carried out at the density functional theory (DFT) with the B3LYP functional and the 6-31G(d) and 6-31+G(d,p) basis sets employing the Gaussian 98 program package.[5] In order to verify the reliability of the presented DFT calculations, all the stable structures were reoptimized at the Møller−Plesset (MP2) levels of theory, and it was found that the optimized geometries do not differ significantly from the structures obtained at the DFT level. Vibrational frequencies of the normal modes for the complexes were calculated at the B3LYP/6-31G(d) level; reported vibrational frequencies are scaled by the standard scaling factor of 0.96.[6]

Results and Discussion

The main parameter by which thermoresponsivity of PEA can be tuned is the degree of neutralization α. It is defined as a ratio of molar concentration of a neutralization base (NaOH in our case) to molar monomer concentration of the polyacid and is related to the degree of ionization of the polymer. Given the concentration used (~16 g/kg), the macroscopic phase separation at ambient temperature was observed by decreasing α from α = 1.0 down to at α = 0.12 (ref 1, Figure 3). A successful preparation of nanoparticles was achieved by heating a solution with α = 0.21. The effect of the degree of neutralization α on the self-assembly behavior of PEA upon heating is shown in Figures 1 and 2.

Figure 1 shows the development of a benzene-normalized scattering intensity, which is proportional to the apparent molecular weight of resulting polymeric nanoparticles. As expected on the basis of our premises, solutions with higher degrees of neutralization show weaker effect upon heating since they are more distant from the critical α corresponding to the macroscopic phase separation. At α = 0.319, no effect is seen upon heating at all. On the other hand, at the lowest α used (α = 0.15)

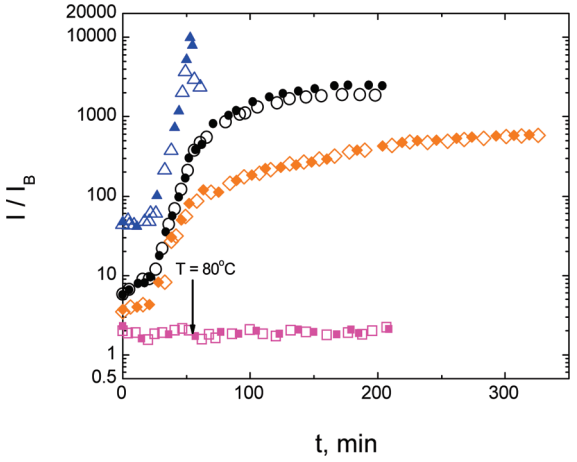

Figure 1. Effect of the degree of neutralization α on the self-assembly behavior of PEA upon heating. Polymer concentration was c = 16 g/kg. Solutions were heated from T = 25 °C to T = 80 °C at the heating rate 1 °C/min and then kept at T = 80 °C. Scattering angles 90° (open symbols) and 45° (closed symbols), respectively. α = 0.150 (△), 0.214 (○), 0.250 (◇), and 0.319 (□). Increase of scattering intensity is due to the irreversible formation of polymeric nanoparticles. Intensities shown are excess intensities (solvent contribution subtracted) and are normalized to benzene scattering I_B.

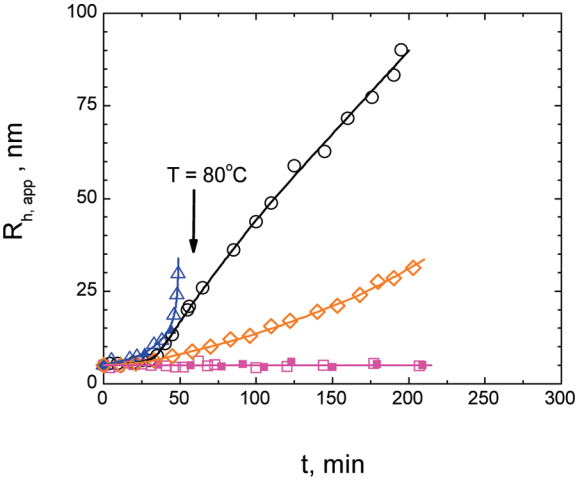

Figure 2. Growth of polymeric nanoparticles upon heating. Dependence on the degree of neutralization α. $R_{h,app}$ is apparent hydrodynamic radius of nanoparticles. Other parameters are the same as in Figure 1.

a very strong and prompt effect was observed, resulting in a very rapid and significant increase of scattering intensity and a large ratio $I(45°)/I(90°)$, both due to arising of rapidly growing large aggregates. The interval of α values at which the aggregation effect is seen corresponds to pH values spanning from 5.25 to 5.90.

Figure 2 shows DLS data. The hydrodynamic radius during heating is calculated only approximately and is denoted as $R_{h,app}$ (apparent). Nevertheless, the DLS data coincide with the above outlined scenario: the growth of nanoparticles is inversely proportional to the degree of neutralization α. We note that a somewhat similar effect of heat-induced aggregation is observed in some protein solutions.[7,8] The mechanism is though different: proteins denature upon heating, and the "sticky groups" otherwise buried inside get on the protein surface and mediate aggregation.

The heat-induced irreversible formation of PEA nanoparticles was further monitored by differential scanning calorimetry. Calorimetric data are shown in Figures 3 and 4. Figure 3 shows

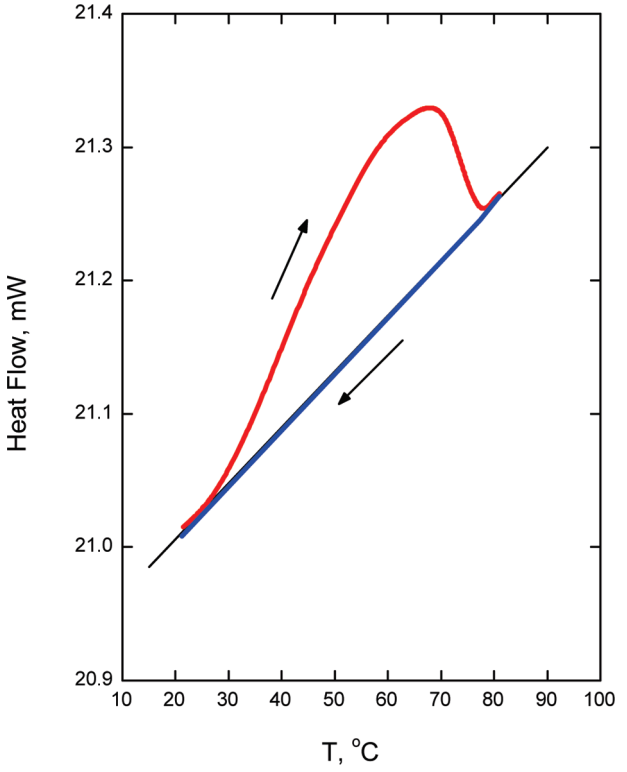

Figure 3. Differential scanning calorimetry (DSC) data on a PEA solution, $\alpha = 0.21$, $c = 16$ g/kg, $c_s = 127$ mM NaCl. Measurements in the standard DSC mode were performed with a constant heating rate 1 °C/min in the heating and cooling runs.

results from a measurement in the standard DSC mode with a constant heating rate 1 °C/min in heating and cooling runs. The most typical sample used in our work ($c = 16$ g/kg, $\alpha = 0.21$) was scanned in the temperature interval from 21 to 81 °C. Two distinct features are found: (i) the transition is one-way (fully irreversible), and (ii) the transition is rather broad, starting around $T = 40$ °C and reaching maximum between 50 and 70 °C. Calorimetric data thus confirm main results from light scattering concerning the irreversibility and a broad (slow) transition upon heating.[1] A minor difference is that the maximum effect in light scattering is seen at a somewhat higher temperature interval compared to DSC. This comes from the different physical principles of both methods. While DSC reflects energetic changes, light scattering reflects structural changes at relatively larger length scales. These can be delayed since energetic and structural changes are consecutive effects.

Figure 4 shows a thermogram recorded during heating and subsequent holding of the sample at elevated temperature, exactly as in the case of the nanoparticle preparation process. The endotherm during heating is followed by a steady increase of heat flow in the hold regime, which is an indication of a continuing endotherm process. This is in full agreement with light scattering data which show that the self-assembly process continues also in the hold regime. The enthalpy change during the endotherm process in Figure 3 was $\Delta H = 41$ J/g; however, it should be noted that the polymer has not fully undergone the transition as shown by Figure 4.

In order to elucidate forces behind the irreversibility of the process of nanoparticle formation, we carried out FTIR measurements. In order to avoid a strong contribution of H_2O to IR spectra, all measurements were done in D_2O solutions. This substitution has no effect on the PEA self-assembly as checked by separate light scattering measurements. FTIR spectra shown in Figure 5 were measured on the most typical solution used in

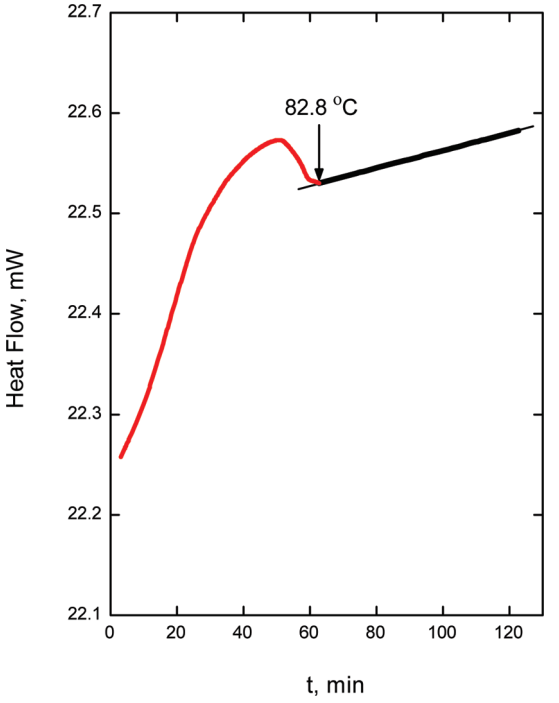

Figure 4. Differential scanning calorimetry (DSC) data upon heating (red line) and subsequent holding of the solution at elevated temperature $T = 82.8$ °C (black line). PEA, $\alpha = 0.21$, $c = 16$ g/kg, $c_s = 127$ mM NaCl. Heating rate 1 °C/min.

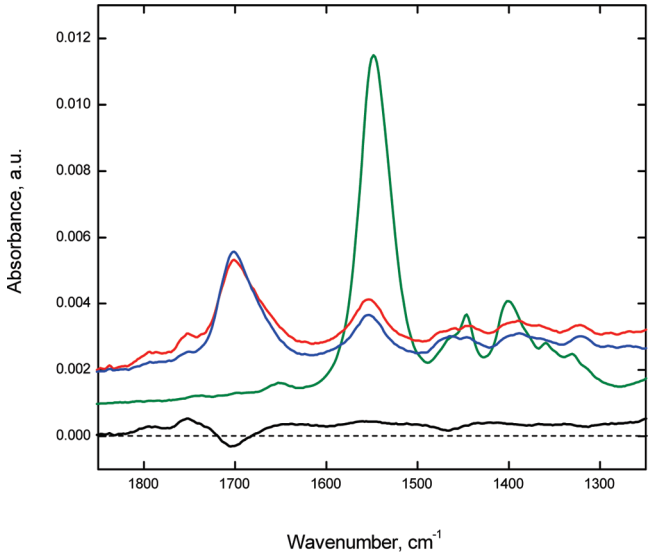

Figure 5. FTIR spectra. PEA, $\alpha = 0.21$, $c = 16$ g/kg, $c_s = 127$ mM NaCl prior to heating (blue line) and after heating according to the usual heating scheme from Figure 1 (red line). PEA, $\alpha = 1.0$, $c = 20$ g/kg (green line). Difference spectrum (black line): spectrum after heating − spectrum before heating. All spectra were acquired in D_2O solutions. The spectrum of D_2O was subtracted.

these studies, which was selected as optimum for the nanoparticle formation, i.e., PEA in 0.12 M NaCl, $\alpha = 0.21$, $c = 16$ g/kg.

Spectra were accumulated prior to heating and after heating according to the usual heating scheme from Figure 1. For comparison, solution with the degree of neutralization $\alpha = 1.0$ (fully neutralized polymer) was also measured. The bands at 1549 and 1401 cm^{-1} correspond to the asymmetric stretching and symmetric stretching vibrations of the free (nonbonded) COO^- groups. These bands dominate the spectra of the sample with $\alpha = 1.0$ while their intensity is strongly decreased in the spectra of

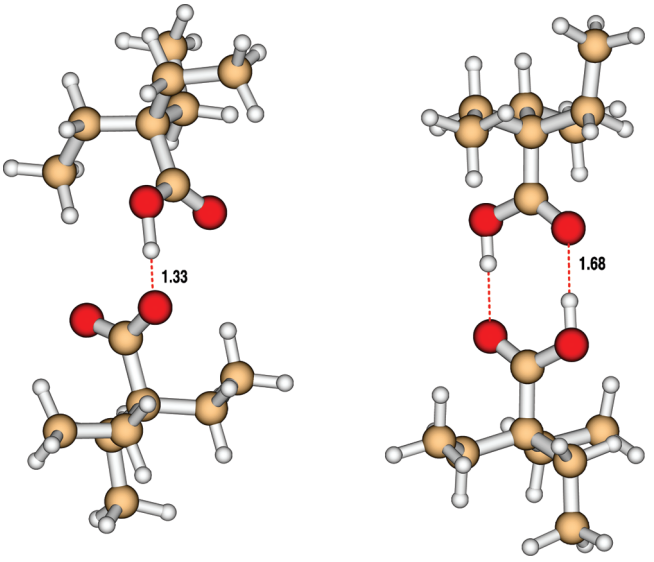

Figure 6. Optimized geometries of the model structures calculated at the B3LYP/6-31G(d) level; distance in angstroms.

the sample with $\alpha = 0.21$. The band at 1549 cm^{-1} is also shifted to 1554 cm^{-1}. From the difference between intensities of the bands at 1549 cm^{-1} at $\alpha = 1.0$ and 1554 cm^{-1} at $\alpha = 0.21$ it can be estimated that compared to $\alpha = 1.0$ only about 13% of the COO^- groups remain free non-hydrogen-bonded at the degree of neutralization $\alpha = 0.21$.

In the spectrum of the sample with $\alpha = 0.21$ a new band is detected at 1702 cm^{-1}. It is assigned to the carbonyl stretching vibration in the COOH group bound in the dimer COOH···COOH, eventually hydrated (DFT calculated frequency of the hydrogen-bonded structure shown in Figure 6 is 1696 cm^{-1}). The intensity of this band decreases after heating, while the intensity of weak bands at 1752 and 1650 cm^{-1} increases, as can be well seen in the difference spectrum. The appearance of the doublet at 1752 and 1650 cm^{-1} is connected with the emergence of hydrogen bonds COOH···COO^-, and the doublet is assigned to the strongly coupled stretching vibrations of the carbonyls in the COOH and COO^- groups. The assignment is supported by DFT calculations of vibrational frequencies in the hydrogen-bonded structure shown in Figure 6: 1747 and 1681 cm^{-1}.

In the spectrum of solution at $\alpha = 1.0$, very weak bands are seen at 1745 and 1653 cm^{-1}. These two bands are obviously analogous to the doublet 1752 and 1650 cm^{-1} detected at $\alpha = 0.21$, and their presence indicates formation of hydrogen bonds COOH···COO^- even in the solution at $\alpha = 1.0$, which thus cannot be fully neutralized.

The band at 1795 cm^{-1} in the solution with $\alpha = 0.21$ is assigned to the carbonyl stretching vibrations of free, nonbonded COOH groups. The free COOH groups are probably buried inside compact structures of PEA, where they cannot form hydrogen bonds due to the sterical hindrance. The intensity of this band and hence the fraction of such free COOH groups slightly increase after heating. This is in agreement with the expected PEA compactization upon heating. In conclusion, FTIR measurements suggest that the main stabilization forces responsible for the irreversibility of the self-assembly are hydrogen bonds, especially COOH···COO^- bonds, which have significantly higher interaction energies compared to COOH···COOH bonds (see results of quantum-chemical calculations in Table 1).

The comparison of cases PMA, PEA, and PPA[1] (PMA being poly(methacrylic acid) and PPA being poly(propylacrylic acid)) is in agreement with these results. Temperature-induced PMA phase segregation occurs at conditions of suppressing the

Table 1. Interaction Energies ΔE (in kcal/mol) and Changes of Gibbs Free Energies ΔG_{298} (in kcal/mol) for the Hydrogen-Bonded Intermolecular Complexes of the Model Structures of PEA (Figure 6)[a]

	COOH···COO^-		COOH···COOH	
method	ΔE	ΔG	ΔE	ΔG
B3LYP/6-31G(d)	−30.2	−19.9	−19.1	−6.5
B3LYP/6-31+G(d,p)	−24.2	−14.7	−15.7	−2.8
MP2/6-31G(d)	−32.1		−18.8	
MP2/6-31+G(d,p)	−28.5		−17.6	

[a] The intermolecular interaction energy was calculated as the difference between the energy of the complex and energies of the separated species.

polymer ionization by HCl addition, and therefore predominantly COOH···COOH bonds may form, not the stronger COO^-···COOH bonds. Therefore, the segregation is reversible, although a very thorough insight into PMA segregation by light scattering[1] shows that some small traces of irreversibility are seen even in the case of PMA, but this is definitely not comparable to full irreversibility in PEA just because of above-mentioned reasons.

A short comment should be added regarding the possibility of monitoring the hydration of COOH groups by hydrogen bonding of water molecules. COOH groups hydrogen bonded with water manifest in a FTIR spectrum via the carbonyl stretching vibration which is at nearly the same frequency as the carbonyl stretching vibration in the COOH group bound in the dimer COOH···COOH. So the two cases cannot be distinguished (both bands at ~1700 cm^{-1}). The experimentally observed peak at 1702 cm^{-1} containing potentially both contributions *decreased* after a heat cycle. On the other hand, peaks corresponding to the formation of COOH···COO^- bonds increased.

Another factor in the stabilization of nanoparticles that needs to be taken into account are entropic forces due to solvent release. Both hydrogen bonds and hydrophobic interactions lead to polymer dehydration and consequently to a higher translational entropy of released water molecules. We expect that the main force leading to the self-assembly is hydrophobic aggregation while hydrogen bonding accompanied by solvent release is mainly a subsequent stabilizing mechanism. Nevertheless, it cannot be excluded that hydrogen bonding may play partly also an active role in the compactization of polymers into assemblies. This was suggested at the level of intramolecular association (two-step intramolecular collapse of chains, where the first step is driven by hydrophobic interactions while the second one by hydrogen bonding).[9] Our older results on irreversible aggregation of ionized (very weakly hydrophobic) PMA are also consistent with this assumption.[10] Hydrogen bonding in general is known for its strong cooperative effects.

A very detailed investigation was performed over past decade on the association behavior of poly(*N*-isopropylacrylamide) (PNIPAM) and its copolymers.[11−29] This thermosensitive (but nonionic) polymer undergoes intramolecular collapse when heated to its demixing temperature, and except for very dilute solutions individual globules also associate into multichain aggregates called mesoglobules. These mesoglobules do not grow infinitely but rather attain a finite size. No macroscopic phase separation (precipitation) occurs; the demixing process ends at a mesoscopic level. In this respect similarity with the system presented in this work is clear. The main difference is, however, that only hysteresis is seen in PNIPAM solutions; i.e., mesoglobules "dissolve" upon cooling back to laboratory temperature. Calorimetric data on PNIPAM show an endotherm upon heating followed by an exotherm upon cooling.[18,19,25] The difference between the aggregation onset and the mesoglobule dissolution in the heating/cooling cycle is only a few degrees. Another substantial difference is that the size distribution of mesoglobules at elevated temperatures above LCST is an equilibrium

distribution, i.e., does not change with time. Our nanoparticles are rather kinetically trapped, and their size distribution depends on incubation time. There are also further dissimilarities regarding morphology of particles. These are important not only because this morphology is a result of the mechanism of particles formation and stabilization but the morphology of particles can also determine backward these mechanisms. Mesoglobules are dense particles with density $\rho \sim 0.4$ g/mL, in contrast to densities of PEA nanoparticles $\rho \sim 0.02$ g/mL. The ratio R_g/R_h in the case of mesoglobules is ~0.8, which is close to the theoretical ratio for homogeneous spheres (0.775). The fractal dimension reported for mesoglobules[23] was $d_f = 2.7$, somewhat smaller than the value $d_f = 3.0$ for homogeneous spheres. In the case of PEA nanoparticles, $R_g/R_h \sim 1.0$ and the fractal dimension $d_f = 2.0$. The comparison of these parameters shows that while PNIPAM mesoglobules are dense, but not fully packed structures, PEA nanoparticles are rather loose structures. Various mechanisms were proposed to account for the stability of PNIPAM mesoglobules. It was suggested that adsorbed traces of ions on the surface of intrinsically neutral mesoglobules may be sufficient to prevent mesoglobule aggregation.[26] The sterical stabilization via a shell of dangling chains which remain partly hydrated upon heating was also considered.[27] The hysteresis was ascribed to protein-like hydrogen bonds between the carbonyl and the amide group ⟩C═O···H−N⟨ based on FTIR measurements.[12,28] An absence of hysteresis in the intramolecular collapse of poly(*N*,*N*-diethylacrylamide) (PDEAM) with no hydrogen donor site[29] supports the importance of hydrogen bonds. The existence of mesoglobules was theoretically predicted based on pure thermodynamic consideration for amphiphilic (competing hydrophobic/hydrophilic) copolymers of various internal monomer distributions, but not for *homo*polymers in bad solvents.[30]

Wu introduced a viscoelastic effect on the stability of the mesoglobular phase,[15,16] which was previously overlooked and which can overwrite thermodynamics and lead to metastable, but very stable mesoglobules. This effect rests on the ineffectiveness of collisions between mesoglobules and chains due to the fact that the contact time upon collision τ_c is shorter than the time required to establish permanent chain entanglements between them τ_e (chain relaxation time). When $\tau_c \ll \tau_e$, the two colliding mesoglobules behave like small elastic nonadhesive "glass" balls. The previously overlooked viscoelastic effect means that aggregates can be stabilized not only by decreasing τ_c, which is directly proportional to the range of hydrophobic interaction and inversely proportional to diffusion coefficient or mean thermal velocity of aggregates, but also by increasing τ_e, which is dependent on polymer molecular weight M, the average polymer concentration inside aggregates ϕ_p, monomer length l_m, and monomer diffusion coefficient D_m, $\tau_e \sim M^3\phi_p^{3/2}l_m^2D_m^{-1}$ (refs 15 and 16). Thus, the increased hydrophobicity of chains leads to better stabilization of aggregates and hence to smaller and more stable aggregates, contrary to conventional expectations. Similarly, the increased rate of heating does, just because of increasing τ_e and simultaneously decreasing τ_c.[15,16] In our system, it is difficult to unambiguously evaluate the influence of the viscoelastic effect since increasing hydrophobicity (lowering α) is accompanied by decreasing charge (suppressing the electrostatic effect). Increased hydrophobicity alone may lead (via viscoelastic effect) to smaller particles. On the other hand, decreased charge promotes aggregation because electrostatic repulsion between particles and polymers is suppressed. As experimental data show, the electrostatic effect seems to prevail. Decreasing α leads to larger and less stable aggregates (Figures 1 and 2). Similarly, increasing the rate of heating does not lead to smaller particles.[1] PEA nanoparticles are rather loose structures due to electrostatic repulsion between charges (much lower ϕ_p, quite different from that in the partially vitrified PNIPAM mesoglobules). Also, the molecular weight of PEA used is rather low. Thus, the viscoelastic effect seems to be not such effective compared to the electrostatic effect. Importantly, it should be noted that long-range electrostatic interactions may significantly modify the entanglement mechanism in a hardly predicting manner given the limited understanding of highly charged and strongly interacting polyelectrolytes. It should be also recalled that our nanoparticles are rather kinetically trapped than being a result of some metastable equilibrium. Given the ionization degree of PEA, there is on average one charged monomer per four uncharged, which is a rather high charge density and the ionic character of PEA must be seriously taken into account.

While the critical behavior and kinetics of the phase separation of water insoluble nonpolar polymers can be characterized as well studied and understood subjects,[31−37] the critical behavior of water-soluble uncharged polymers (especially PNIPAM and its copolymers) is currently studied in detail as discussed above; the critical behavior of charged polymers is virtually unexplored. Muthukumar et al.[38] investigated experimentally the phase separation kinetics of polyelectrolyte solutions with a conclusion that it follows an entirely different law from what is expected in systems of uncharged polymers. A challenge was posed with respect to extending the current theories of phase separation kinetics to charged systems.[38] This is surely a nontrivial task taking into account the complicated nature of polyelectrolytes and many types of specific effects. In the absence of an adequate theory we will discuss only qualitatively which types of effects can be possibly brought into consideration due to the polyelectrolyte character of the polymer. In contrast to nonionic polymers, two opposing forces are simultaneously engaged: attractive hydrophobic interaction due to poor solvent and repulsive electrostatic interaction, both on intra- and intermolecular level. The presence of neutralizing counterions as a third component is also crucial. The macroscopic phase separation is disfavored due to a large entropic penalty caused by an accompanying redistribution of counterions. It was suggested that because of this reason, the macroscopic phase separation into dilute and concentrated phases is not the only option and that weakly charged polyelectrolytes in poor solvents may minimize the entropy loss associated with counterions redistribution by formation of microphase separation: alternating regions with high and low polymer densities.[39,40] Counterions as a third component also drastically influence the situation by condensation on chains and their aggregates. This condensation is concentration and conformation dependent.[41,42] The coupling of condensation to conformation may lead to a chain collapse accompanied by a drastic reduction of charge due to an avalanche type of counterion condensation.[43,44] Condensed counterions not only screen charges but also create ion pairs and may result in attractive interactions (thermally averaged monopole−dipole and dipole−dipole interactions). Charge fluctuations on surfaces of charged chains and charged aggregates may generate electrostatic attractive interactions, too.[45−47] Another specific effect related to the polyelectrolyte nature of the polymer is the Rayleigh instability of charged chains and aggregates. According to the classical problem of the instability of a charged droplet considered by Lord Rayleigh,[48] a charged droplet is unstable and breaks into smaller droplets above a critical charge value. Applying this idea, a necklace-like conformation of hydrophobic polyelectrolytes was predicted based on analytical theory[49] and simulations.[50] Compact beads comprised of folded parts of chain are supposed to be joined by narrow strings of elongated parts of chains. At the prevalence of hydrophobicity over intramolecular electrostatic repulsion (due to higher hydrophobicity, lower charge density or higher screening at high concentrations) chains are supposed to collapse into single globules instead of forming stable necklaces. The question at which conditions the necklace-like chain

structure may be observed is currently intensively discussed. The Rayleigh instability on a level of aggregates of charged chains may act against aggregation.[41]

Most works in the field of hydrophobic polyelectrolytes is focused on single-chain properties (dilute solutions). Many-chain problems and detailed analysis of the phase behavior are addressed much more scarcely. Analytical theory treats the phase separation without discrimination between macroscopic and mesoscopic separation.[49] Many-chain problems were treated by MD simulations in a salt-free system.[50,51] The simulation without explicit solvent[50] yielded neither phase separation nor aggregation but instead stable single-chain globules (at relatively high concentrations comparable to those used in this work). On the other hand, considering explicit solvent[51] yielded quite different result: once the solvent-induced interaction is strong enough to collapse a single chain, aggregation or phase separation always occurs.[52]

Let us now discuss how the above-mentioned polyelectrolyte effects may take part in our PEA system. Regarding the counterion condensation, its onset in solutions of a similar polyelectrolyte (poly(methacrylic acid)) was found[53] in agreement with the Manning criterion at $\alpha \sim 0.36$. Therefore, we may assume that we are below the counterion condensation threshold. The avalanche counterion condensation effect upon heat-induced chain compactization is apparently not present since resulting nanoparticles are still moderately charged as revealed by zeta potential measurements. A large entropic penalty due to counterions redistribution associated with a macroscopic phase separation may be one of the factors leading to the preference of mesoscopic phase separation over macroscopic (in addition to the stabilization of mesoscopic aggregates by electrostatic repulsion). The comparison[1] of cases PMA, PEA, and PPA fully supports this notion. Thermoresponsivity of PMA is achieved at conditions of suppressed charges (low pH, very low amount of dissociated counterions) and results in a macroscopic phase separation upon heating. On the other hand, thermoresponsivity of PEA and PPA occurs at conditions of relatively high charge densities (large amount of dissociated counterions) and results in a mesoscopic phase separation. Regarding the Rayleigh instability of a charged PEA complex, we expect that it is overwhelmed by hydrogen bonding acting in an opposite direction. Regarding the Rayleigh instability on a level of individual chains leading possibly to a necklace-like chain structure, no conclusion is possible given the available data. Since our current data show that PEA nanoparticles are loose structures, the following scenarios can be considered: (i) Relatively swollen chains associate (possibly necklace-like, then most probably via beads, which are less charged compared to strings). (ii) Collapsed single-chain globules associate such that form branched structures (branched garlands of globules[54]). The specificity of our system is that we do not deal with a weakly charged hydrophobic polyelectrolyte, which is mostly discussed in polyelectrolyte literature, but with a strongly charged hydrophobic polyelectrolyte. The nature of the phase transition is therefore different.

The role of charges in PEA nanoparticles stabilized by cooling down to ambient temperature was further investigated via a pH titration. Figure 7 shows data obtained upon titration of a dilute solution of nanoparticles (c = 0.033 g/L, salt concentration c_s = 2.5 mM NaCl) with HCl and NaOH, respectively. Solution pH prior to the titration was pH = 6.2.

The titrant was added slowly to the analyte by a syringe pump to adjust pH, and then the measurement was performed after ca. 25 min of equilibration. The apparent hydrodynamic radius R_h was obtained via the Stokes−Einstein relation from a diffusion coefficient measured at scattering angle 173°. More technical details can be found in the experimental part. R_h was found to be pH-independent within experimental scatter in the range

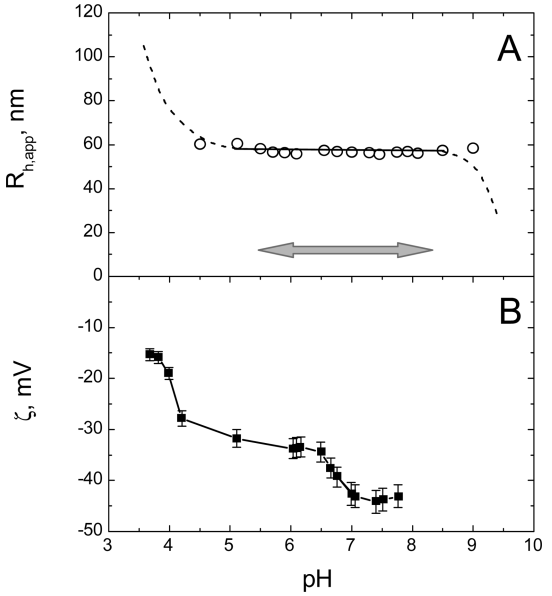

Figure 7. Stability of PEA nanoparticles with respect to solution pH. $R_{h,app}$ is apparent hydrodynamic radius. ζ is zeta potential. The dashed line corresponds to multimodal spectra of relaxation times. The arrow indicates pH interval corresponding to α values from α = 0 to α = 1.0. Concentration c = 0.033 g/kg.

pH = 4.5−7.3. At pH < 4.5, an apparent increase of R_h is seen while at pH > 7.3 an apparent decrease is observed. Since these are only apparent changes in R_h, they are presented by a dashed line. The real situation is more complex and is exactly documented in Figure 8, which shows size distributions obtained from spectra of relaxation times by Laplace inversion. Upon decreasing pH by HCl addition, an aggregation process is evident, which manifests itself in the appearance of a separate peak corresponding to aggregates, which are up to 10 times larger than original PEA nanoparticles. These large aggregates coexist with smaller aggregates yielding a polydisperse population. The size distribution of these aggregates gradually shifts to larger sizes up to pH = 3.02. The polymer then macroscopically separates from solvent below this pH. The reason for the aggregation of PEA particles is evident from Figure 7B, which shows a decreasing absolute value of zeta potential by lowering pH. While the dominant process at low pH is aggregation of individual PEA particles, the dominant process in the limit of high pH (pH > 7.3) is a gradual disintegration of PEA particles. Three peaks appear in the size distribution. While the peak corresponding to the original size of nanoparticles is persisting to high pH, two new peaks appear: one in the range of several nanometers and one in the range of ∼500 nm. While the former peak corresponds to individual chains (or dimers, possibly trimers, etc.), the latter one corresponds to larger aggregates which arise probably as a result of linking several PEA particles during the process of their disintegration. Size distributions in Figure 8 are so-called intensity distributions, which means that peak areas correspond to the intensities of light scattered by corresponding scatterers, not weight fractions or number fractions of scatterers. This means that while the peak corresponding to individual chains is small, the weight fraction of individual chains in solution is already dominant. On the other hand, the weight fraction of larger aggregates, which accompany the process of disintegration of PEA nanoparticles, is very small. Similarly to DLS data, radii of gyration obtained by SLS in the interval pH = 4.5−7.3 where monomodal distributions are obtained yield also no dependence on pH (not shown). Other polymeric structures (micelles, microgels) based on poly(carboxylic acid)s exhibit in contrast a pH-dependent size. Increase of pH (increase of degree of ionization)

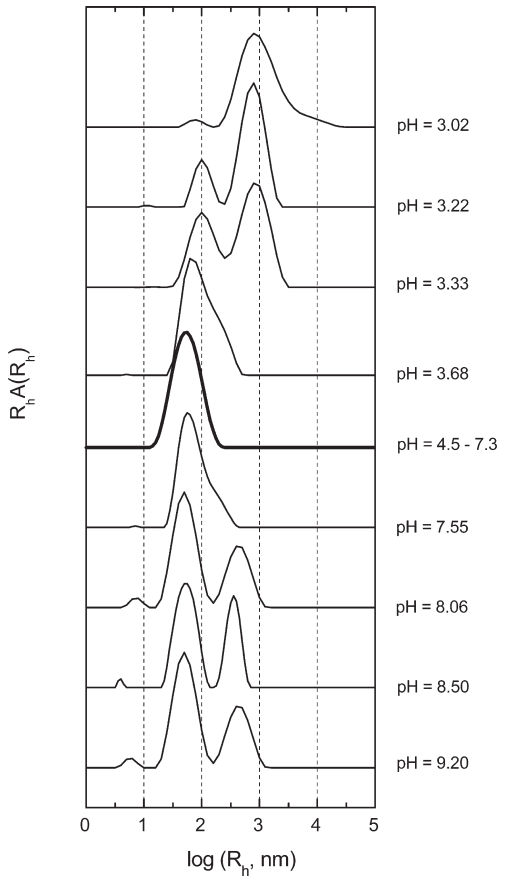

Figure 8. Spectra of relaxation times obtained from dynamic light scattering experiments on solutions of PEA nanoparticles. pH was adjusted by additions of NaOH or HCl. $c = 0.033$ g/kg. Scattering angle $\theta = 173°$.

causes swelling due to increasing repulsive interactions between charges. The absence of swelling in the case of PEA nanoparticles arises most probably from the nature of the mechanism of their stability. Increasing the number of COO^- groups should cause stronger repulsive interactions but on the other hand may result also in increased hydrogen bonding, which acts in the opposite direction. The absence of swelling as well as finally the disintegration of nanoparticles upon charging of carboxylic groups supports the notion that hydrogen bonds are responsible for the nanoparticles stability upon completing a heating cycle.[55]

Nanoparticles are stabilized by hydrogen bonds and presumably also by frozen-in hydrophobic interactions between polymer molecules. This reminds the stabilization of globular proteins. These are known to be denatured by means of urea addition. The exact role of urea in the denaturation process on a molecular level is still under debate;[56] nevertheless, its function in terms of the final result is clear. In order to test our conclusions about the stabilization forces, urea was added to solutions of PEA nanoparticles. Figure 9 shows a summary of these types of experiments. While no effect was seen at low urea concentrations (up to ~300 mM) a very clear process of particle disintegration ("denaturation") can be monitored in real time at high urea concentrations. An example obtained at 3.49 M urea concentration is shown in Figure 9. The decaying scattering intensity is reflecting the decreasing molecular weight of particles during their disintegration. At urea concentrations between 300 mM and 3.49 M the strength of the disintegration effect is proportionally lower and its kinetics is slower.

Nanoparticles were also tested with respect to the stability in saline solutions of various concentrations and found to be stable

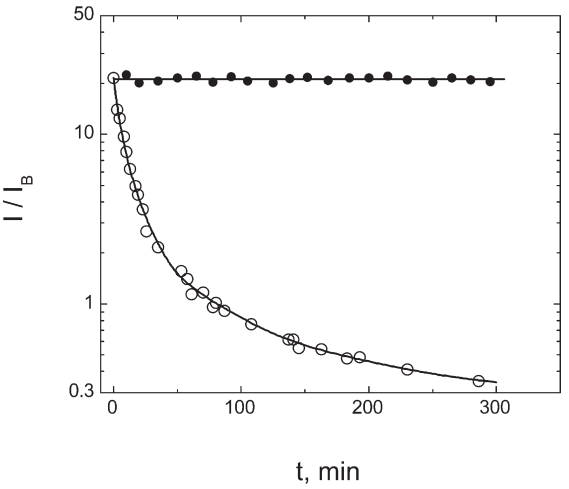

Figure 9. Effect of urea addition on the stability of PEA nanoparticles. Urea concentration 260 mM (●) and 3.49 M (○). Polymer concentration $c = 0.1$ g/kg. Disintegration of particles is reflected in a decrease of scattering intensity, which is proportional to their molecular weight. Intensities shown are excess intensities (solvent contribution subtracted) and are normalized to benzene scattering I_B.

from deionized water up to 0.6 M NaCl, i.e., including physiological salt concentration (0.15 M NaCl).

Conclusions

Heat-set poly(ethylacrylic acid) nanoparticles were investigated in detail by a combination of light scattering techniques, differential scanning calorimetry, and FTIR spectroscopy. While the driving force for the particle formation is of thermodynamic origin, due to decreasing solvent quality with temperature, the irreversibility of the particle formation is achieved by the stabilization of nanoparticles via hydrogen bonds, mainly $COOH\cdots COO^-$. The full irreversibility of the process was confirmed also by differential scanning calorimetry. The stabilization of nanoparticles by hydrogen bonds and presumably also by frozen-in hydrophobic interactions resembles the stabilization of globular proteins. Similarly in the case of proteins the PEA nanoparticles are denatured by urea. The advantage of the ionic nature of the polymer for the creation of nanoparticles is twofold: First, charged COO^- groups are stronger HB acceptors compared to COOH and are capable of creation of stronger bonds as revealed also by our quantum-chemical calculations on the concrete molecular architecture. Second, the overall charge on growing nanoparticles prevents their coagulation, leading otherwise to macrophase separation. It is expected that a similar approach could be used also for other polymers. Successful experiments on the most relative polymer (poly(propylacrylic acid)) are in progress. In general, the criteria for applicable polymers are that they can yield a thermosensitive polymer−solvent system and are capable of self-hydrogen-bonding. Charges on chains are advantageous since they contribute to the stabilization of nanoparticles.

Acknowledgment. Support of the Research and Development Agency of the Slovak Republic (Grant No. 51-037905), Slovak grant agency VEGA (grant No. 2/6197/26), and Action COST D43 is acknowledged. Č.K. acknowledges support from the Grant Agency of the Czech republic (Grant No. 202/09/2078). Authors are also thankful to A. Sikora for DSC measurements and to E. Gyöngyösiová for technical assistance. This work was realized within the frame of the project "Centre of Excellence for Advanced Materials with Nano- and Submicron Structure", which is supported by the Operational Program "Research and

Development" of the Slovak republic financed through European Regional Development Fund.

References and Notes

(1) Sedlák, M.; Koňák, Č. *Macromolecules* **2009**, in press. DOI: 10.1021/ma9015032.
(2) Provencher, S. W. *Comput. Phys. Commun.* **1982**, *27*, 213–227.
(3) Jakeš, J. *Czech. J. Phys.* **1988**, *38*, 1305.
(4) Štěpánek, P. In *Dynamic Light Scattering. The Method and Some Applications*; Clarendon: Oxford, 1993; Chapter 4.
(5) Frisch, M. J.; Trucks, G. W.; Schlegel, H. B.; Scuseria, G. E.; Robb, M. A.; Cheeseman, J. R.; Montgomery, Jr., J. A.; Vreven, T.; Kudin, K. N.; Burant, J. C.; Millam, J. M.; Iyengar, S. S.; Tomasi, J.; Barone, V.; Mennucci, B.; Cossi, M.; Scalmani, G.; Rega, N.; Petersson, G. A.; Nakatsuji, H.; Hada, M.; Ehara, M.; Toyota, K.; Fukuda, R.; Hasegawa, J.; Ishida, M.; Nakajima, T.; Honda, Y.; Kitao, O.; Nakai, H.; Klene, M.; Li, X.; Knox, J. E.; Hratchian, H. P.; Cross, J. B.; Bakken, V.; Adamo, C.; Jaramillo, J.; Gomperts, R.; Stratmann, R. E.; Yazyev, O.; Austin, A. J.; Cammi, R.; Pomelli, C.; Ochterski, J. W.; Ayala, P. Y.; Morokuma, K.; Voth, G. A.; Salvador, P.; Dannenberg, J. J.; Zakrzewski, V. G.; Dapprich, S.; Daniels, A. D.; Strain, M. C.; Farkas, O.; Malick, D. K.; Rabuck, A. D.; Raghavachari, K.; Foresman, J. B.; Ortiz, J. V.; Cui, Q.; Baboul, A. G.; Clifford, S.; Cioslowski, J.; Stefanov, B. B.; Liu, G.; Liashenko, A.; Piskorz, P.; Komaromi, I.; Martin, R. L.; Fox, D. J.; Keith, T.; Al-Laham, M. A.; Peng, C. Y.; Nanayakkara, A.; Challacombe, M.; Gill, P. M. W.; Johnson, B.; Chen, W.; Wong, M. W.; Gonzalez, C.; Pople, J. A. *Gaussian 03, Revision C.02*; Gaussian, Inc.: Wallingford, CT, 2004.
(6) Scott, A. P.; Radom, L. *J. Phys. Chem.* **1996**, *100*, 16502.
(7) Pouzot, M.; Nicolai, T.; Durand, D.; Benyahia, L. *Macromolecules* **2004**, *37*, 614–620.
(8) Mehalebi, S.; Nicolai, T.; Durand, D. *Soft Matter* **2008**, *4*, 893–900.
(9) Vallat, P.; Catala, J. M.; Rawiso, M.; Schosseler, F. *Europhys. Lett.* **2008**, *82*, 28009-p1−6.
(10) Sedlák, M.; Koňák, Č.; Štěpánek, P.; Jakeš, J. *Polymer* **1990**, *31*, 253–257.
(11) Qiu, X.; Kwan, C. M. S.; Wu, C. *Macromolecules* **1997**, *30*, 6090.
(12) Cheng, H.; Shen, L.; Wu, C. *Macromolecules* **2006**, *39*, 2325–2329.
(13) Peng, S.; Wu, C. *Polymer* **2003**, *44*, 1089–1093.
(14) Siu, M.; Liu, H. Y.; Zhu, X. X.; Wu, C. *Macromolecules* **2003**, *36*, 2103–2107.
(15) Zhang, G.; Wu, C. *Adv. Polym. Sci.* **2006**, *195*, 101–176.
(16) Wu, C.; Li, W.; Zhu, X. X. *Macromolecules* **2004**, *37*, 4989–4992.
(17) Ye, J.; Xu, J.; Hu, J. M.; Wang, X. F.; Zhang, G. Z.; Liu, S. Y.; Wu, C. *Macromolecules* **2008**, *41*, 4416–4422.
(18) Qiu, X. P.; Tanaka, F.; Winnik, F. M. *Macromolecules* **2007**, *40*, 7069–707.
(19) Kujawa, P.; Aseyev, V.; Tenhu, H.; Winnik, F. M. *Macromolecules* **2006**, *39*, 7686–7693.
(20) Balu, C.; Delsanti, M.; Guenoun, P. *Langmuir* **2007**, *23*, 2404–2407.
(21) Vallat, P.; Catala, J. M.; Rawiso, M.; Schosseler, F. *Europhys. Lett.* **2008**, *82*, 28009-p1–28009-p6.
(22) Dawson, K. A.; Gorelov, A. V.; Timoshenko, E. G.; Kuznetsov, Yu. A.; Chesne, A. Du. *Physica A* **1997**, *244*, 68–80.
(23) Aseyev, V.; Hietala, S.; Laukkanen, A.; Nuopponen, M.; Confortini, O.; Du Prez, F. E.; Tenhu, H. *Polymer* **2005**, *46*, 7118–7131.
(24) Kujawa, P.; Tanaka, F.; Winnik, F. M. *Macromolecules* **2006**, *39*, 3048–3055.
(25) Ding, Y. W.; Ye, X. D.; Zhang, G. Z. *Macromolecules* **2005**, *38*, 904.
(26) Chan, K.; Pelton, R.; Zhang, J. *Langmuir* **1999**, *15*, 4018–4020.
(27) Vasilevskaya, V. V.; Khalatur, P. G.; Khokhlov, A. R. *Macromolecules* **2003**, *36*, 10103–10111.
(28) Maeda, Y.; Higuchi, T.; Ikeda, I. *Langmuir* **2000**, *16*, 7503–7509.
(29) Zhou, K.; Lu, Y.; Li, J.; Shen, L.; Zhang, G.; Xie, Z.; Wu, C. *Macromolecules* **2008**, *41*, 8927–8931.
(30) Timoshenko, E. G.; Kuznetsov, Yu. A. *J. Chem. Phys.* **2000**, *112*, 8163–8175.
(31) Wiltzius, P.; Bates, F. S.; Heffner, W. R. *Phys. Rev. Lett.* **1988**, *60*, 1538.
(32) Stepanek, P.; Lodge, T. P.; Bates, F. S. *J. Chem. Phys.* **1991**, *94*, 8289.
(33) Lal, J.; Bansil, R. *Macromolecules* **1991**, *24*, 290.
(34) Balsara, N. P.; Lin, C.; Hammouda, B. *Phys. Rev. Lett.* **1996**, *77*, 3847.
(35) Kojima, J.; Takenaka, M.; Nakayama, Y.; Hashimoto, T. *Macromolecules* **1999**, *32*, 1809.
(36) Hayashi, M.; Jinnai, H.; Hashimoto, T. *J. Chem. Phys.* **2000**, *113*, 3414.
(37) Lefebvre, A. A.; Lee, J. H.; Balsara, N. P.; Vaidyanathan, C. *J. Chem. Phys.* **2002**, *117*, 9063.
(38) Kanai, S.; Muthukumar, M. *J. Chem. Phys.* **2007**, *127*, 1–14.
(39) Borue, V. Y.; Erukhimovich, I. Y. *Macromolecules* **1988**, *21*, 3240–9.
(40) Joanny, J. F.; Leibler, L. *J. Phys.* (*Paris*) **1990**, *51*, 545–57.
(41) Manning, G. S. *Macromolecules* **2007**, *40*, 8071–8081.
(42) Muthukumar, M. *Macromolecules* **2004**, *120*, 9343.
(43) Khokhlov, A. R. *J. Phys. A: Math. Gen.* **1980**, *13*, 979–987.
(44) Klooster, N.; van der Touw, F.; Mandel, M. *Macromolecules* **1984**, *17*, 2070.
(45) Ray, J.; Manning, G. S. *Langmuir* **1994**, *10*, 2450–2461.
(46) Khalatur, P. G.; Khokhlov, A. R.; Mologin, D.; Reineker, P. *J. Chem. Phys.* **2003**, *119*, 1232–1247.
(47) Although not used in our work, we also note that multivalent counterions lead to collapse and/or aggregation and/or phase separation by effects of bridging, specific adsorption and displacing of monovalent counterions, neutralization, or even polyion charge reversal.
(48) Rayleigh, Lord *Philos. Mag.* **1882**, *14*, 182.
(49) Dobrynin, A. V.; Rubinstein, M. *Prog. Polym. Sci.* **2005**, *30*, 1049–1118.
(50) Micka, U.; Holm, C.; Kremer, K. *Langmuir* **1999**, *15*, 4033–4044.
(51) Chang, R.; Yethiraj, A. *Chem. Phys.* **2003**, *118*, 6634–6647.
(52) The polymer-poor phase is almost pure solvent while the polymer-rich phase comprises of an aggregate in which all chains from the simulation box are aggregated. Authors conclude that these aggregates represent a macrophase separation since when the simulation was performed with a larger simulation box with more chains, the size of the aggregate increased as well. We note, however, that the number of chains in the box was only 64. For comparison, our aggregation numbers in PEA nanoparticles are on the order of 2000. We note also the difference that we have salt in the system.
(53) Sedlák, M.; Koňák, Č.; Štěpánek, P.; Jakeš, J. *Polymer* **1987**, *28*, 873–880.
(54) Maresov, E. A.; Semenov, A. N. *Macromolecules* **2008**, *41*, 9439–9457.
(55) If the particles would be cross-linked by some types of covalents bonds, this would not be observed.
(56) Stumpe, M. C.; Grubmüller, H. *J. Am. Chem. Soc.* **2007**, *129*, 16126–16131.